

# EXPERIMENTAL CONDITIONS TO ACCESS HIGH-PERFORMANCE H-MODE PLASMAS WITH SMALL ELMS AT LOW COLLISIONALITY IN JET-ILW

E. DE LA LUNA<sup>1</sup>, M. DUNNE<sup>2</sup>, P. LOMAS<sup>3</sup>, C. REUX<sup>4</sup>, E. R. SOLANO<sup>1</sup>, J. GARCÍA<sup>4</sup>, M. FAITSCH<sup>2</sup>, M. PORADZINSKI<sup>3</sup>, G. PUCCELLA<sup>6</sup>, S. MENNUIR<sup>3</sup>, R. COELHO<sup>5</sup>, B. LABIT<sup>7</sup>, O. SAUTER<sup>7</sup>, E. VIEZZER<sup>8</sup>, M. WISCHMAIER<sup>2</sup>, JET CONTRIBUTORS\* AND THE EUROFUSION TOKAMAK EXPLOITATION TEAM<sup>†</sup>

<sup>1</sup>Laboratorio Nacional de Fusión, CIEMAT, 28040, Madrid, Spain

<sup>2</sup>Max-Planck-Institute for Plasma Physics, D-85748, Garching, Germany

<sup>3</sup>United Kingdom Atomic Energy Authority, Culham Science Centre, OX14 3DB, Abingdon, UK

<sup>4</sup>CEA, IRFM, F-13108, Saint Paul-lez-Durance, France

<sup>5</sup>Instituto de Plasmas e Fusão Nuclear, IST, Universidade de Lisboa, 1049-001, Lisboa, Portugal

<sup>6</sup>ENEA, Fusion and Nuclear Safety Department, 00044, C.R. Frascati (Roma), Italy

<sup>7</sup>Ecole Polytechnique Federale de Lausanne, Swiss Plasma Center, CH-1015, Lausanne, Switzerland

<sup>8</sup>Department of Atomic, Molecular and Nuclear Physics, University of Seville, 41012, Seville, Spain

\* See the author list of “Overview of T and D-T results in JET with ITER-like wall” by CF Maggi et al. to be published in Nuclear Fusion Special Issue: Overview and Summary Papers from the 29th Fusion Energy Conference (London, UK, 16-21 October 2023)

† See the author list of “Progress on an exhaust solution for a reactor using EUROfusion multi-machines capabilities” by E. Joffrin et al. to be published in Nuclear Fusion Special Issue: Overview and Summary Papers from the 29th Fusion Energy Conference (London, UK, 16-21 October 2023).

First author e-mail address: [elena.delaluna@ciemat.es](mailto:elena.delaluna@ciemat.es)

## Abstract

Significant progress in establishing quasi-stationary conditions for a high fusion performance regime at low  $q_{95}$  ( $=3.2$ ) with very small ELMs has been realized in recent JET experimental campaigns. Operationally, access to such a regime is enabled by using high NBI power on a low-density target at high plasma current (3 MA/2.8T), achieved by completely removing the gas injection. This operating regime combines the desired properties of good H-mode energy confinement ( $\beta_N=1.8-2.2$ ) and no core W accumulation with small ELMs at low pedestal collisionality ( $v_{e,ped}^* \sim 0.1$ ), similar to that expected in ITER. Due to the lower recycling and wall retention of the Be-wall, lower pedestal densities can be achieved in JET-ILW, which allows access to a low-density regime that was not accessible with the C-wall. This small ELMs regime simultaneously achieved values of beta, safety factor and edge collisionality relevant for the ITER baseline scenario, which distinguish it from other small ELM regimes, typically explored at high  $q_{95}$  and higher pedestal collisionality. The edge plasma in the small ELMs regime exhibits high-temperature pedestal profiles and a wide pedestal density profile with a shallow gradient, similar to that observed in the I-mode. However, in contrast to observations in the I-mode, no edge coherent MHD activity (WCM in I-mode) is detected in JET. Pedestals are found to be stable to peeling-ballooning modes, consistent with the lack of large ELMs. The recipes used to access and maintain the regime will be presented, and the operational limits encountered will be discussed.

## 1. INTRODUCTION

Investigating scenarios with high energy confinement and no or small ELMs is of continuing importance in fusion research. There are two main reasons to give priority to such research. Firstly, the large transient heat flux associated with type I ELMs must be avoided in ITER and future fusion reactors in order to avoid excessive damage to the plasma-facing components. Secondly, since ITER will operate with a W divertor, the control of the W concentration to avoid its accumulation in the core region is mandatory to achieve ITER’s performance. It is well known that ELMs play a key role in regulating the particle and impurity transport at the plasma edge. Therefore, a better understanding of the physics mechanisms leading to impurity control in the absence of ELMs is also of great importance for ITER. The ability to produce small ELMs while at the same time maintaining the good confinement properties of the H-mode is an important step needed to achieve the ITER  $Q=10$  goal. This has triggered a major experimental effort in many other tokamaks world-wide aimed at exploring and better understanding operation regimes with small ELMs. Different small ELMs regimes, such as grassy ELMs [1,2], QCE [3] or the EDA [4,5], have been discovered and are being investigated in JET and many other tokamaks worldwide. However, accessing small ELMs in the ITER baseline scenario ( $H_{98}=1$ ,  $\beta_N=1.8$ ,  $\beta_{pol}<1$  and  $q_{95}\sim 3$ ) at reactor-relevant conditions, such as low collisionality, is very challenging and much of the work in recent years has focused on exploring scenarios at high  $q_{95}$  ( $> 4$ ) and high collisionality [6]. In this paper, we follow a different

route, a high-performance H-mode regime ( $H_{98} \geq 1$  and  $\beta_N = 1.8-2$ ) at low  $q_{95} = 3.2$  and low pedestal collisionality ( $\nu_{e,ped}^* \sim 0.1$ ) with small ELMs discovered during the 2019 campaign in JET [7,8]. The new regime has two noteworthy characteristics: first, it combines high fusion performance with small ELMs, which significantly reduces the transient heat loads driven by ELMs into the divertor; and second, no core W accumulation is observed. Since these experiments were carried out using the baseline scenario, we will refer to it as the ‘Baseline Small ELMs’ (BSE) regime to highlight the region of the operational parameter space that it occupies, which distinguishes it from other small ELMs regimes. Initial experiments were presented at the 2021 IAEA conference [8]. Motivated by these initial results, further exploration of the BSE regime was carried out in the summer of the 2023 campaign as part of a recent experimental effort in JET to investigate and better understand small ELMs regimes. The recent experiments had two main goals: (1) extending the operational experience of the unfuelled BSE scenario, particularly towards achieving longer stationary periods, and (2) identifying the mechanisms involved in accessing small ELMs at low collisionality.

## 2. GENERAL CHARACTERISTICS OF THE HIGH FUSION PERFORMANCE PLASMAS WITH SMALL ELMs AT LOW COLLISIONALITY

The experiments reported here were conducted using the same engineering parameters as the initial experiments in 2019: a plasma current ( $I_p$ ) of 3 MA, a magnetic field ( $B_T$ ) of 2.8 T, resulting in  $q_{95} = 3.2$ , and a low triangularity ( $\delta_{ave} \sim 0.2$ ), lower single null plasma shape with both strike points placed in the divertor corners for optimum pumping, and with the ion  $\nabla B$  drift direction favourable for H-mode access, which is the workhorse for the baseline studies in JET-ILW. High neutral beam injection (NBI) power (19-25 MW) combined with up to 3-5 MW of ion cyclotron resonant heating power (ICRH, H minority heating), was applied on a low-density plasma, achieved by completely removing the gas injection.

One of the limitations of the initial experiments done in 2019 was that the discharges were transient in nature. Although the density and radiation remained pretty constant during the no-gas phase, the ion temperature ( $T_i$ ) and the neutron rate did not reach a steady state and continuously rose during the high-performance phase. In 2023, careful adjustment of the NBI power during the entry to H-mode at high gas and the use of higher NBI power have enabled discharge reproducibility and the extension of the plasma duration. In these new discharges, the phase with very small ELMs was extended up to 3.3 s (1.5-2 s in 2019), allowing not only the density but also temperature profiles to reach quasi-stationary conditions for up to  $\sim 1.3$  s. An example of such behaviour is shown in Fig. 1, where the confinement properties of the no-gas BSE regime are compared with the conventional gas fuelled ELMy H-mode under similar conditions. The plasma evolution during the initial phase of the discharge is very similar for both discharges. The transition to H-mode is followed by the appearance of type I ELMs that arrest the density rise and allow the plasma density to reach a stationary behaviour. The density remains constant for the duration of the heating phase in the gas fuelled plasma, but it significantly dropped at  $t = 8.8$  s in the case of #103833, following the removal of the external gas dosing. With the decrease in density, the plasma enters a

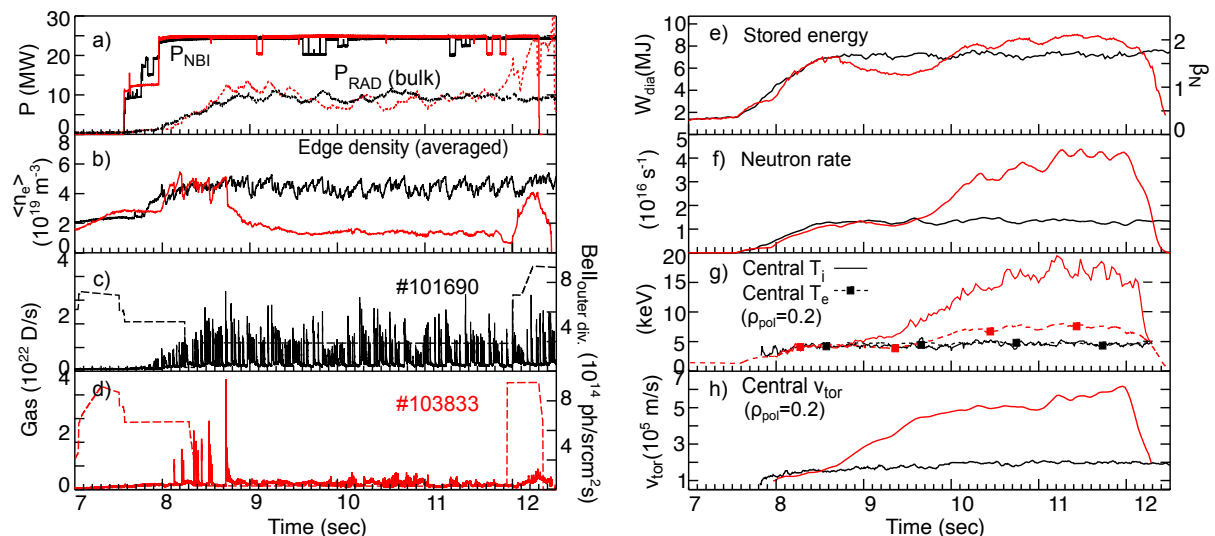


Fig. 1: Comparison of two baseline plasmas (3 MA,  $q_{95} = 3.2$ , low  $\delta$ ) in JET-ILW: #101690 (type I ELMs), with gas fuelling and pellet pacing, and #103833 (small ELMs), without external gas dosing during the main heating phase. The plasma terminated in a disruption triggered by radiative edge cooling starting at  $t = 11.9$  s.

phase with very small ELMs that lasts till the end of the no-gas phase. The impact of the small ELMs on the fast stored energy signal is within the signal noise level ( $\Delta W_{\text{ELM}} < 30$  kJ), resulting in an averaged ELM energy loss normalized to the pedestal energy  $< 3\%$ .

In Fig. 2, the profiles for density, temperature, and toroidal rotation for #103833 at three times are compared: a time during the initial ELMy H-mode phase at  $t \sim 8.7$  s (pre-ELM), at  $t = 9$  s coinciding with the maximum on the bulk radiated power ( $P_{\text{RAD}}^{\text{bulk}}$ ), and a time during the high fusion performance phase at  $t \sim 11.5$  s. Density profiles are obtained from Thomson scattering (TS) measurement, TS and electron cyclotron emission (ECE) provide  $T_e$  data, while  $T_i$  and rotation are measured with charge exchange recombination spectroscopy (CXRS). Dramatic peaking of the electron density, ion temperature and rotation is observed following the removal of the gas injection. In the absence of external gas fuelling, the NBI heating provides the only source of neutrals in the central plasma region, thus leading to a strong peaking of the density profile, owing to the central deposition obtained with such low edge densities. Operation at low edge density leads to relatively high electron ( $T_e$ ) and ion ( $T_i$ ) temperatures, reaching core  $T_i$  values above 15 keV, with  $T_i/T_e \sim 2$  starting from the pedestal region, and strong plasma rotation. Pedestal densities ( $n_{e,\text{ped}}$ ) as low as  $1.85 \times 10^{19} \text{ m}^{-3}$  and  $T_{e,\text{ped}} > 1.6$  keV, with  $T_{i,\text{ped}} > 4$  keV, have been achieved. In such conditions, low pedestal collisionality ( $\nu_{e,\text{ped}}^* \sim 0.1$ ) is reached [8], which is amongst the lowest values achieved in JET-ILW and is similar to the range expected in ITER. Previous gyrokinetic analyses have shown that the improved core energy confinement obtained in such a regime is facilitated by favourable conditions for ion temperature gradient (ITG) driven turbulence stabilisation [7,8].

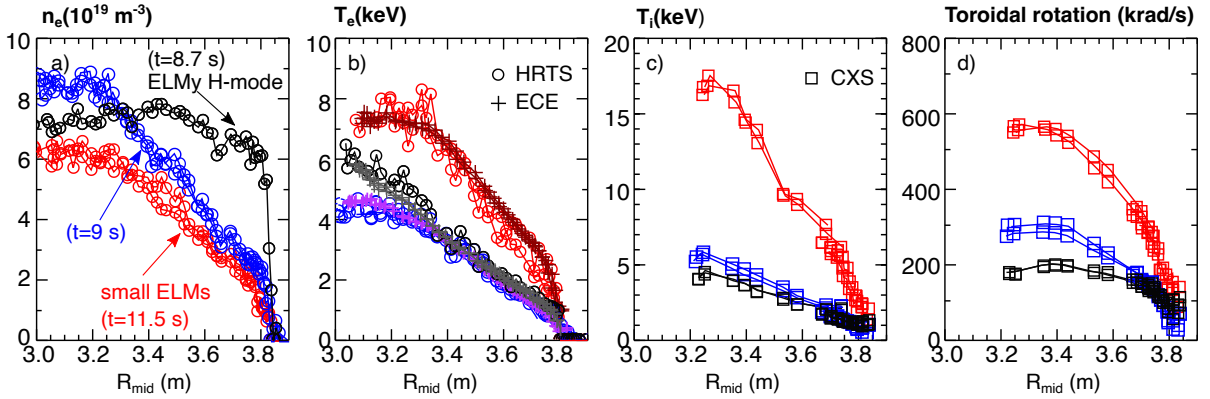


Fig. 2: Density, electron and ion temperature, and toroidal rotation profiles in the ELMy H-mode and the no-gas phase with small ELMs for the same discharge shown in Fig. 1. It also includes a time during the low-performance phase ( $t=9$  s) after the removal of the gas injection. (Note the scale for  $T_i$  is twice that of the  $T_e$ ).

During the phase with small ELMs, the edge density and  $P_{\text{RAD}}^{\text{bulk}}$  remain stationary, indicating that the particle and impurity transport is not increasing in the absence of large ELMs. In these conditions, the radiation remains localized at the midplane on the outboard side of the poloidal cross-section, which is a common feature of JET discharges dominantly heated by NBI. In this example, a degradation of the energy confinement is observed during the initial phase of the discharge. Between  $t=9$  and  $9.4$  s the  $T_e$  in the central region decreases by 30%, causing the stored energy to drop (see Fig. 1(e)). Note that this does not affect the rotation build up in the core region. The available measurements indicate that this is associated with an increase in the core radiation driven by the high density peaking achieved during this phase (shown in Fig. 2). After  $t=9.4$  s, central  $T_e$  steadily increases, and at  $t=10.2$  s, the plasma enters a phase with excellent energy confinement (with  $\beta_N \geq 1.8$ ), as evidenced by the higher values for the plasma stored energy (7MJ in #101690 compared to 9.2 MJ in #103833) and the neutron yield obtained, compared to the conventional ELMy H-mode discharge. This high-performance phase lasts  $\sim 1.3$  s in quasi-stationary conditions, corresponding to more than 5 energy confinement times. No signs of core accumulation are observed during the high-performance phase, demonstrating that W control is possible despite the absence of regular type I ELMs and the sizeable density peaking reached in these discharges. Gyrokinetic calculations [7] have shown that the observed behaviour is consistent with the dominance of neoclassical transport for high-Z impurities in the central region. In addition to the well-known candidates affecting the neoclassical convection, such as the  $n_i$  and  $T_i$  gradients, it was found that plasma rotation plays a crucial role in ensuring good W screening by causing a reversal of the neoclassical convection direction from inward to outward, consistent with the lack of core accumulation observed in the no-gas BSE regime. Recent modelling results have further corroborated the beneficial effects of plasma rotation in the impurity transport via enhanced temperature screening

strength at low collisionality [9]. In this case, the pre-programmed discharge termination was initiated at  $t=11.9$  s with a large D gas injection. Unfortunately, this coincides with a sudden increase in the outboard radiation that contributes to a global rise in the total radiated power, alerting the tokamak protection system, which issues an interlock switching off the NBI power at  $t=12.3$  s. The important issue of the limits affecting the duration of the high confinement phase is discussed in section 3.

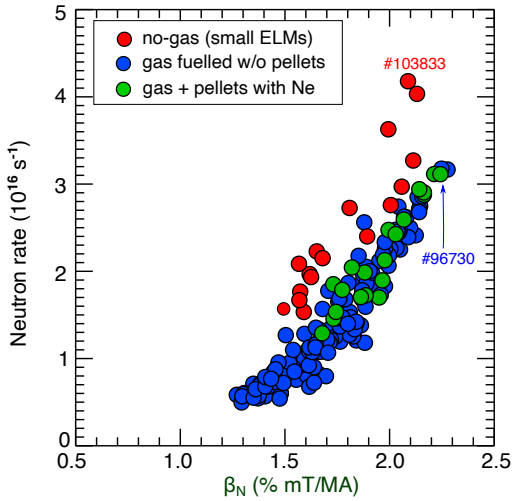


Fig. 3: Neutron rate versus  $\beta_N$  for a JET-ILW dataset at 3 MA ( $q_{95}=3.2$ , low  $\delta$ ) that includes unfuelled, gas fuelled with and without pellets, and with and without Ne injection ( $\Gamma_{Ne} < 2 \times 10^{22}$ ).

The combination of high density and high  $T_i$  in the plasma core leads to high neutron rates for these discharges, as seen in Fig. 1(f). Notably, the BSE discharge shown in Fig. 1 produced the highest ( $\sim 4.2 \times 10^{16} \text{ s}^{-1}$ ) fusion yields from deuterium plasmas achieved, so far, in the baseline scenario in JET-ILW. This is illustrated in Fig. 3, where the neutron rate (averaged over  $\geq 0.5$  s) is plotted versus normalized beta ( $\beta_N = \beta / (I_p / a B_T)$ ) for a dataset of unfuelled BSE discharges at 3 MA, along with a comprehensive dataset of ELMy H-mode discharges with the same  $I_p / B_T$  and plasma shape. The ELMy H-mode database includes gas-fuelled discharges with/without pellet pacing and with/without Ne injection ( $\Gamma_{Ne} < 3 \times 10^{22} \text{ s}^{-1}$ ) and covers a wide range of plasma parameters:  $5 < \bar{n}_e (10^{19} \text{ m}^{-3}) < 8.5$ ,  $15 < P_{NBI} (\text{MW}) < 30$  and  $1.0 < P_{ICRH} (\text{MW}) < 5.0$ . The best performance in the gas fuelled baseline scenario was obtained using low gas injection and pellet pacing [10], which allowed access to higher pedestal and core temperatures while keeping core radiation under control.

In this scenario, the stored energy remained stationary for up to 5 s. It was found that Ne injection at levels low enough for the divertor to remain attached, allowed access to lower plasma density and improved confinement [11]. One can see that, for the same  $\beta_N$  (or stored energy), higher neutron rates are obtained for the unfuelled BSE discharges, indicating the improved core confinement of the no-gas BSE regime. We note that the previous neutron rate record of  $\sim 3.2 \times 10^{16} \text{ s}^{-1}$  was obtained in a discharge at higher NBI power ( $P_{IN}=32.8$  MW for #96730 compared to 27.1 MW for #103833). Generally, good agreement between the measured and simulated neutron rate values using TRANSP is found for the baseline scenario [12]. In the case of #103833, the TRANSP analysis shows that  $\sim 60\%$  of the neutrons during the high fusion performance phase are produced by thermal reaction, while the rest is produced mostly by beam-thermal reactions and a small fraction of beam-beam reactions. A prediction of the D-T performance of this discharge, assuming one of the NBI beam boxes in deuterium to be replaced by one using tritium, has been obtained using TRANSP. According to that calculation, a fusion power of  $\sim 9.8$  MW would be obtained.

From previous experiments in JET-C [13], it is known that low density and strong rotation facilitate the creation of a hot ion mode ( $T_i > T_e$ ). With the C-wall, careful attention to wall conditioning to reduce recycling was a prerequisite to prepare the low-density target needed to access a hot ion regime. The novelty of the present results is that the experiments in JET-ILW combine the high-performance properties of a hot ion core with no or very small ELMs that last for up to 3 s, while in JET-C, the hot ion was basically an ELM-free H-mode, where plasma density and radiation rose continuously increased and therefore had a limited duration ( $< 1.7$  sec), typically terminated by a large ELM or a radiative collapse.

## 2.1 Operational space diagram

The good confinement in the no-gas BSE scenario results primarily from the ability to operate at low density. Using the scenario shown in Fig. 1, pedestal electron densities as low as  $1.85 \times 10^{19} \text{ m}^{-3}$  and  $T_{e,ped} > 1.6$  keV have been achieved, thus significantly expanding the operational space of H-mode plasmas in JET at 3 MA. This is illustrated in Fig. 4, where the pedestal parameters for baseline plasmas at 3 MA with and without gas dosing are compared. The figure also includes data from H-mode plasmas with no gas dosing at 3 MA ( $\delta=0.25$ ,  $q_{95}=3.1$ ), in JET with the carbon wall (JET-C), which contrary to the observations in JET-ILW, are typically characterised by low-frequency large type I ELMs ( $f_{ELM}=8-15$  Hz). The  $T_e$ - $n_e$  diagram has been built using the pedestal height obtained from 'modified tanh' fits of the TS data, using multiple profiles selected within stationary time windows

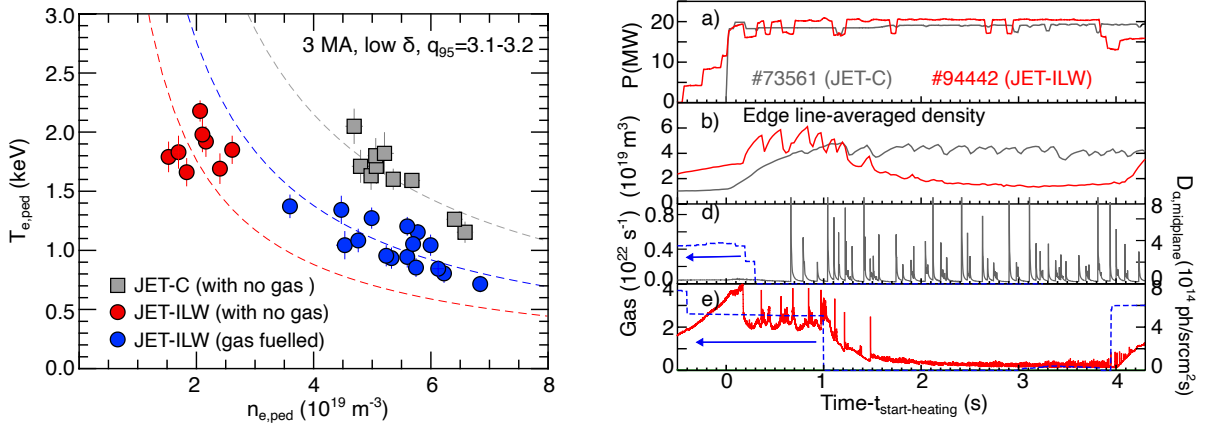


Fig. 4: (left) Pedestal top values for electron temperature and density for a baseline dataset (3 MA,  $q_{95}=3.1-3.2$ , low  $\delta$ ) including JET-C and JET-ILW discharges with and without gas external dosing. Dashed curves represent contours of constant electron pressure. (right) Comparison of 2 discharges without gas dosing during the main heating phase and similar heating power in JET-C (gray) and in JET-ILW (red).

of 0.5 s during the main heating phase. The data is taken during the phase with the highest performance in all cases. As expected, the pedestal density is higher, and the temperature is lower in the gas-fuelled discharges in JET-ILW. The discharges with the lowest  $n_{e,ped}$  in that dataset were run using low gas ( $\Gamma_D < 10^{22}$  D/s), pellet pacing and Ne seeding. Interestingly, the ‘natural’ plasma density, defined as the density achieved in an H-mode discharge with beam fuelling and no external gas puffing, is found to be significantly higher in the C-wall discharges, about twice that seen in JET with the Be/W-wall. The impact of the wall materials on the edge density and ELM behaviour is clearly seen in Fig. 4 (right column), where a pair of discharges without gas fuelling and similar NBI power are compared. The lower achievable pedestal densities in JET-ILW can be explained by the lower recycling and wall retention of the Be-wall, which allows access to a low-density regime that was not accessible with the C-wall, thus explaining why this small ELM regime was not discovered sooner.

### 3. ROLE OF MHD ACTIVITY AND DURATION OF THE HIGH FUSION PERFORMANCE PHASE

Operation at low density and low  $q_{95}$  gives rise to various MHD activity. An example of such activity can be seen in the spectrogram plotted in Fig. 5 for the same discharge shown in Fig. 1. Typically, the high fusion performance phase in the no-gas BSE discharges is largely sawtooth-free and dominated by continuous modes with  $n=1$  toroidal number and sporadic fishbones, indicating that the central  $q$  ( $q_0$ ) is in the vicinity of 1, but not low enough to produce sawteeth. In the example shown in Fig. 5, a long-lasting continuous  $n=1$  mode at 30 kHz can be seen from 8.4 s onwards, whose frequency evolution is close to that of the central plasma rotation. The possibility that it is an infernal mode cannot be excluded, especially in the hypothesis that  $q_0$  is just about 1 and, therefore, a kink cannot exist. The infernal mode is a pressure-driven instability that can be excited in a region of low magnetic shear [14]. Similar modes have been observed in JET-ILW hybrid plasmas [15]. A small  $m/n=2/1$  ( $m$  is the poloidal mode number) neoclassical tearing mode (NTM) is observed at a lower frequency (16 kHz) that persists for the remainder of the discharge. A short-lived  $5/4$  NTM mode can also be seen at  $t=8.75$  s, triggered by a sawtooth crash. Such mode bursts are often observed in good-performing discharges but do not lead to a significant energy loss ( $\sim 5-10\%$ ). After the power is switched off at  $t=12.3$  s, the  $2/1$  mode starts to grow, and with the plasma rotation decreasing rapidly, it locks, and a disruption occurs.

The rise in the total radiated power responsible for triggering the H-mode termination is due to a dramatic increase in the outboard radiation leading to unacceptable radiative edge cooling. Confirmation that edge cooling initiates the sequence of events leading to the disruption is obtained by examining the evolution of the  $T_e$  profile during the last phase of the discharge ( $t > 11$  s). As shown in Fig. 5(c), a strong modulation can be seen in the  $T_e$  measured by ECE at various radii, affecting the outer plasma region. The effect of such modulation is visible in the  $T_e$  profiles shown in panel (h). The times of the selected profiles are marked by vertical lines on Fig. 5(e-g). The analysis of the experimental observations performed so far suggests that the behaviour of the  $T_e$  profile is the result of the combination of two main effects. The first is a modulation of the edge radiated power ( $P_{RAD}^{edge}$ ), which causes the  $T_e$  in the outer plasma region ( $R_{mid} > 3.5$  m) to drop as the edge radiation rises.  $P_{RAD}^{edge}$  is evaluated by averaging the radiation contained in the edge region with  $0.7 < \rho_{pol} < 0.95$ , obtained from bolometer tomography. As can be seen in Fig. 5(e), this modulation appears to be strongly correlated with the movement of the outer

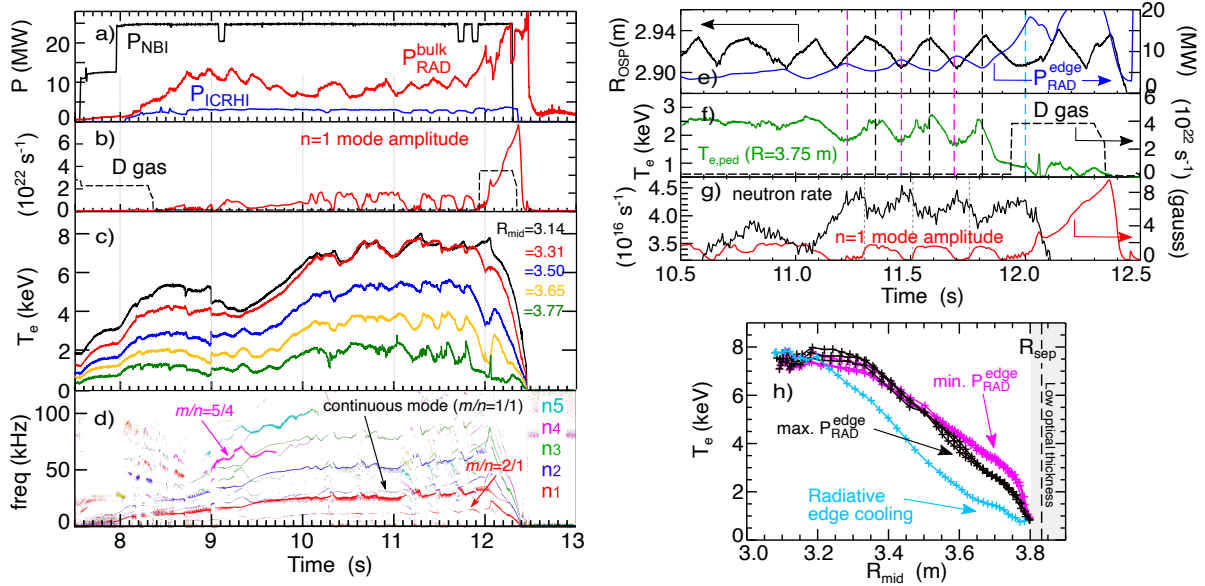


Fig. 5: (left) Time evolution of (a) NBI, ICRH and bulk radiated power, (b) D gas fuelling and  $n=1$  mode amplitude, (c)  $T_e$  at different radii, as measured by ECE, and (d) the spectrogram and toroidal mode number analysis of magnetic data for the same discharge as shown in Fig. 1. An expanded view of the high fusion performance phase is plotted on the right, top panels showing: (e) the position of the outer strike point ( $R_{OSP}$ ), the edge radiation averaged over the region  $0.7 < \rho_{pol} < 0.95$  ( $P_{RAD}^{edge}$ ), (f) the pedestal electron temperature ( $T_{e,ped}$ ) and (g) the neutron rate. The  $T_e$  profile (ECE) at the times marked by vertical lines in the top panels, showing the impact of the edge radiated power modulation and the onset of the edge cooling prior to the disruption.

strike point ( $R_{OSP}$ ). Strike point sweeping at 4Hz over a distance of 3–4 cm was used in these experiments. This is the standard configuration in the JET baseline scenario, motivated by the need to mitigate divertor heat loads when using high NBI power. The second effect is an increase in central temperatures starting at  $t=11.05$ s, as the edge temperature decreases. This is observed for both electrons and ions, as can be seen by the response of the neutron rate. The  $T_e$  increase in the central region is small ( $\sim 5\%$ ), but it appears sufficient to modify the plasma current profile via increased resistivity, causing a modulation of the core  $n=1$  mode amplitude. This MHD perturbation located in the core region is responsible for the oscillations observed in the neutron rate (see Fig. 5(g)). The rise in central temperatures triggered by a rapid cooling at the edge has been observed in many tokamaks [16,17], associated with non-local transport effects typically observed in low-density, high-electron temperature plasmas, as is the case described here. In the example shown in Fig. 5, the collapse of the  $T_{e,ped}$  starts at  $t\sim 11.85$ s (see Fig. 5(f)), but it is further exacerbated by the large peripheral gas injection initiated at 11.95s, which results in higher edge densities, more radiation and lower edge temperatures, leading to the dramatic increase of the edge radiation power and early termination of the discharge. It is worth mentioning that, while all the recent discharges were run using a similar strike point sweeping, the edge radiated power modulation described above is not present in all of them. Initial analysis of the data indicates that the amplitude of the oscillation on  $P_{RAD}^{edge}$  increases with increasing  $T_{e,ped}$  but more work is needed to clarify the correlation and causality between the strike point sweeping and the enhanced edge cooling leading to the disruption.

### 3.1 Operational constraints and remaining challenges

Plasma operation with no gas injection in a metal wall device at low  $q_{95}$  is challenging, and a disruptive plasma termination is a common feature of the no-gas BSE discharges. Plasma in this operating regime terminated in one of two ways: via enhanced edge radiation resulting in edge cooling termination (discussed in the previous section) or due to limits imposed by operation at low density. In the absence of external gas injection, the plasma density strongly depends on the fuelling provided by the NBI. It was found that a minimum NBI power of 22 MW was required to maintain the density above the minimum value needed to fulfil the JET-ILW requirements regarding beam shine-through power loading of in-vessel components. In JET-ILW, the temperature on the surface of Be limiters close to one of the beam boxes is monitored during the entire discharge. In the BES discharges, at low density and high NBI power, this temperature increases steadily during the high-power phase, sometimes reaching the maximum allowable value. This causes the NBI power to switch off prematurely by tripping a fast interlock designed to protect the Be limiters from excessive reionization heat loads. Turning off the NBI power so abruptly

is often followed by disruptions, particularly in low  $q_{95}$  discharges. Operational experience in JET indicates that increasing the outer plasma-wall gap could reduce the incidence of such events, but unfortunately, we did not have time to explore this option.

#### 4. ELM DYNAMICS AND PEDESTAL STRUCTURE

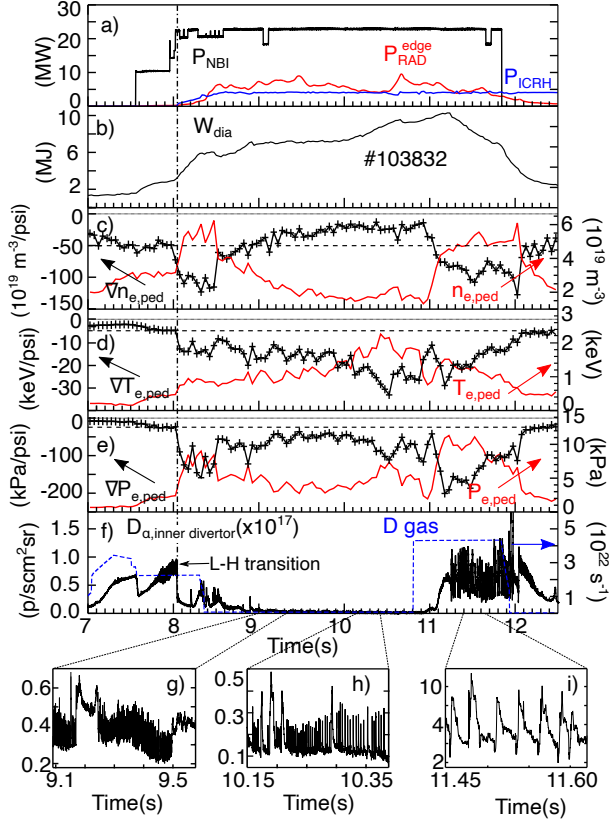


Fig. 6: Time traces for a no-gas BES plasma (#103832) including the pedestal height and maximum gradient for  $n_e$ (c),  $T_e$ (d) and  $P_e$ (e). The  $D_\alpha$  signal (inner divertor) (f) and zooms to selected time windows (g-i) show the remarkable changes in ELM dynamics observed in this operating regime.

Finally, in the later phase of the discharge, the density quickly rises in response to the increase in gas fuelling, the pressure gradient increases and type I ELMs reappear (Fig. 6(i)), settling to a frequency of  $\sim 53$  Hz, which is a clear indication of the important role played by the pedestal density structure in the access to the small ELMs. These observations are consistent with recent L-H transition studies, demonstrating that the no-gas BSE scenario operates in the region where  $P_{LH}$  rises substantially with decreasing density, known as the ‘low-density branch’ of the L-H threshold power. We note that operation with an edge power flow only marginally above  $P_{LH}$  at higher densities (where  $P_{LH}$  increases with plasma density), typically leads to low-quality H-mode with low  $T_{e,ped}$ , which is very different to the situation described here. This is illustrated in Fig. 6(c-e), where the changes in the edge profiles as the plasma transitions from a conventional ELMy H-mode to the small ELMs regime can be seen. The distinctive features are lower pedestal density and shallower density gradient, with higher  $T_{e,ped}$  and  $T_{i,ped}$  (not shown) and stronger temperature gradients, relative to the ELMy H-mode. The combination of a reduced pedestal density gradient and the concomitant decrease in the edge current density makes the edge plasma of the no-gas BSE discharges very stable with respect to the peeling-ballooning modes[8], consistent with the lack of ELMs. It is interesting to note that while the height and the maximum gradient of the  $n_e$  profile reach roughly constant values during the phase with small ELMs, the height and gradient of the pedestal  $T_e$  profile continue increasing, becoming steeper than that in the ELMy H-mode, until this raise is interrupted at  $t=10.5$  s by an increase in the edge radiation. These changes indicate that the edge pedestal profiles are not fixed by MHD stability limits, as in the case of the ELMy H-mode, but are most likely transport limited through a balance between the neoclassical and the turbulence transport. We note that the edge of the no-gas BSE discharges has similarities to that in I-mode,

One puzzling feature of the experimental results shown here is the dramatic change in ELM dynamics with the decrease in edge density as the external gas fuelling is removed. This is visualized in more detail in Fig. 6, where the temporal evolution of the pedestal heights and maximum gradients of the pedestal profiles for  $n_e$ ,  $T_e$  and  $P_e$  is plotted for one of the recent BSE discharges. In this case, the duration of the no-gas phase was shortened to investigate the impact of gas fuelling on the pedestal structure and in the onset of type I ELMs. Note that the plasma lands safely in this example. One can see that with the decrease in edge density, the large ELMs appearing in the initial gas-fuelled H-mode phase are replaced by very small ELMs without degradation of plasma confinement, contrary to what is typically observed in the transition to the so-called ‘low density’ type III ELMs in JET-C[19]. Interestingly, despite the high NBI power applied (with  $P_{sep}/P_{LH}^{ITPA} > 1.5$ , where  $P_{LH}^{ITPA}$  is the ITPA scaling for the H-mode threshold power [18]), the dynamics of the spectroscopy signals measured in the divertor during the no-gas phase resemble that observed during operation close to the H-mode power threshold ( $P_{LH}$ ). This includes H-L-H transition (see Fig. 6(g)) accompanied by an oscillatory behaviour with a frequency of  $\sim 1$  kHz ( $m=1$  and  $n=0$ ) known as M-mode in JET[20]. As the  $T_{e,ped}$  increases, the M-mode activity gradually disappears, and small and fast (up to  $\sim 285$  Hz) ELMs can be identified (Fig. 6(h)).

with H-mode like pedestals in ion and electron temperatures and a weak one in density. Moreover, the I-mode regime is obtained at powers below the L-H power threshold, in conditions where the  $P_{LH}$  is high (unfavourable  $B \times VB$  drift) and the particle and heat transport are found to be decoupled [20,21]. However, in contrast to observations in the I-mode, no edge coherent MHD activity (WCM in I-mode) is detected in the BSE regime. More theoretical and experimental work is needed to identify the mechanism responsible of providing the additional particle transport to maintain the wide pedestal density in the BSE regime, while leaving the energy transport unaffected.

## 5. CONCLUSIONS

A high fusion performance regime at low density and low  $q_{95}$  ( $=3.2$ ) has been investigated in JET, which combines the desired properties of good H-mode energy confinement ( $\beta_N=1.8-2.2$ ) and no core W accumulation with small ELMs at low pedestal collisionality ( $v_{e,ped}^* \sim 0.1$ ). It is worth emphasizing that access to the low pedestal collisionality anticipated in ITER is particularly challenging in metal wall devices, and therefore, the regime developed in JET-ILW provides a valuable platform for pedestal physics studies in conditions where pedestal temperature and density profiles are substantially different from those obtained in conventional ELMy H-mode plasmas. By extending the duration of the no-gas phase, longer phases with small ELMs were achieved (up to  $\sim 3.5$  s), allowing the stored energy and neutron rate to reach quasi-stationary conditions for  $\sim 1-1.5$  s. So far, the duration of the high-performance phase is generally limited by edge radiative cooling or too high head loads on the Be limiters that lead to an uncontrolled early termination of the discharge. As a result, the disruptivity rate is relatively high, which is not surprising since the regime is still in the development phase. We believe further optimization of these results should be possible, considering the small number of no-gas BSE discharges performed thus far on JET.

This small ELMs regime simultaneously achieved values of  $\beta_N$ ,  $q_{95}$  and edge collisionality relevant to the ITER baseline scenario. Outstanding challenges in terms of reactor relevance include low-density operation, with  $f_G \leq 0.4$ , ( $f_G = \bar{n}_e/n_G$ ), with  $n_G = I_p/(\pi a^2)$ ) compared with the ITER baseline scenario  $f_G \sim 0.85$ , and the compatibility with divertor detachment. Nevertheless, this kind of plasma shows that the ELM dynamics and pedestal behaviour in conditions with no or very low particle source (no-gas injection and low recycling) can be very different to those observed in a conventional ELMy H-modes run in machines with C-walls or gas fuelling. This is an especially important topic to investigate since in future fusion devices, like ITER, fuel penetration beyond the separatrix, from gas, edge recycling or even from pellets, will be much weaker than in present devices.

## ACKNOWLEDGEMENTS

This work has been carried out within the framework of the EUROfusion Consortium, funded by the European Union via the Euratom Research and Training Programme (Grant Agreement No 101052200 — EUROfusion). This research was partly supported by grant PID2021- 127727OB-I00 of the Spanish Ministry of Science and Innovation. The Swiss contribution to this work has been funded by the Swiss State Secretariat for Education, Research and Innovation (SERI). Views and opinions expressed are however those of the author(s) only and do not necessarily reflect those of the European Union, the European Commission or SERI. Neither the European Union nor the European Commission nor SERI can be held responsible for them.

## REFERENCES

- [1] Y. KAMADA et al., Plasma Phys. Control. Fusion **42** (2000) A4247 [2] Q. YANG et al., Nuclear Fusion **60** (2020) 076012
- [3] M. FAITSCH et al., Nuclear Materials and Energy **26** (2021) 100890
- [4] M. GREENWALD et al., Physics of Plasmas **6** (1999)1943
- [5] L. GIL et al., Nucl. Fusion **60** (2020) 054003
- [6] E. VIEZZER et al., Nuclear Materials and Energy **26** (2023) 101308
- [7] J. GARCÍA et al., Physics of Plasmas **29** (2022) 032505
- [8] E. DE LA LUNA et al., Submitted for publication in Nuclear Fusion
- [9] D. FAJARDO et al., Plasma Phys. Control. Fusion **65** (2023) 035021
- [10] L. GAZOTTI et al., this conference
- [11] S. GABRIELLINI et al., Nuclear Fusion **63** (2023) 086025
- [12] Z. STANCAR et al., this conference
- [13] THE JET TEAM, Plasma Phys. Control. Fusion **37** (1995) A359
- [14] J. MANICKAM et al., Nuclear Fusion **27** (1987) 1461
- [15] P. BURATTI et al., Nuclear Fusion **52** (2012) 023006
- [16] K. W. GENTLE, et al., Phys. Plasmas **2** (1995) 2292
- [17] M.W. KISSICK et al., Nucl. Fusion **36** (1996) 1691
- [18] Y. R. MARTIN et al., Plasma Phys. Control. Fusion **46** (2004) 7
- [19] E.R. SOLANO et al., Nucl. Fusion **57** (1996) 022021
- [20] D.G WHYTE et al., Nucl. Fusion **50** (2010) 105005
- [21] T. HAPPEL et al., Plasma Phys. Control. Fusion **59** (2017) 014004